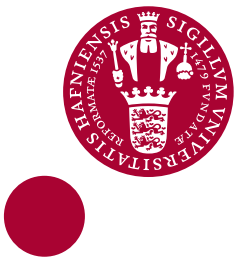

Deterministic Single-Phonon Source Triggered by a Single Photon

Sollner, Immo; Midolo, Leonardo; Lodahl, Peter

Published in:
Physical Review Letters

DOI:
10.1103/PhysRevLett.116.234301

Publication date:
2016

Document version
Publisher's PDF, also known as Version of record

Deterministic Single-Phonon Source Triggered by a Single Photon

Immo Söllner,* Leonardo Midolo, and Peter Lodahl
Niels Bohr Institute, University of Copenhagen, Blegdamsvej 17, DK-2100 Copenhagen, Denmark
(Received 31 January 2016; published 9 June 2016)

We propose a scheme that enables the deterministic generation of single phonons at gigahertz frequencies triggered by single photons in the near infrared. This process is mediated by a quantum dot embedded on chip in an optomechanical circuit, which allows for the simultaneous control of the relevant photonic and phononic frequencies. We devise new optomechanical circuit elements that constitute the necessary building blocks for the proposed scheme and are readily implementable within the current state-of-the-art of nanofabrication. This will open new avenues for implementing quantum functionalities based on phonons as an on-chip quantum bus.

DOI: 10.1103/PhysRevLett.116.234301

Engineering of periodic nanostructures has proven to be an immensely powerful tool to shape the properties of a material. Most notably are photonic crystals, which are created by the periodic modulation of the refractive index. Their photonic band gaps and defect modes have been widely studied [1] and have found a number of applications in nanophotonics. For example, in solid-state quantum optics, they are commonly used to control light-matter interaction [2]. Similarly, the periodic modulation of mechanical properties leads to the formation of phononic crystals [3]. Chip-scale devices that allow engineering of both the photonic and the phononic density of states simultaneously have recently been proposed [4–7]. This has lead to a range of theoretical [8,9] and experimental [10–12] breakthroughs in optomechanics. In parallel, there has been significant progress on coupling single solid-state emitters, in the form of nitrogen-vacancy centers or self-assembled quantum dots (QDs), to mechanical resonators either via magnetic gradient coupling [13,14] or strain coupling [15–21]. Additionally, the potential of using phononic crystals to control single-phonon mediated processes in solid-state systems has recently been alluded to [22,23].

In optics, the reliable generation and detection of single-photon and entangled-photon states has important applications within quantum information science. Similar goals are being pursued in optomechanics where the generation [12,24–26] and detection [11] of nonclassical phononic states are opening new avenues of research. These schemes are typically probabilistic and rely on the direct radiation-pressure interaction between colocalized optical and mechanical modes where the coupling rate between the modes is proportional to the square root of the intracavity photon number [27]. However, parasitic absorption is a problem for large intracavity photon numbers when operating at millikelvin temperatures [12,28], which becomes necessary when performing experiments on single phonons with frequencies in the few gigahertz (GHz) regime. In this Letter, we propose an alternative approach based on a hybrid optomechanical (OM) crystal where we engineer the coupling of a three-level emitter to both the photonic and the phononic reservoirs. We demonstrate how the internal spin state of the emitter can be used to mediate strong photon-phonon interaction for an emitter embedded in the OM crystal. In contrast to the standard approach in optomechanics [11,24–27], our proposal does not rely on radiation-pressure coupling, which is strong for large intracavity photon numbers. Instead, the deterministic single-photon–single-phonon cascade triggered by a single narrow-bandwidth photon is operated at an average intracavity photon numbers significantly below one [29], thus offering a route to circumvent the problem of parasitic heating. We propose a readily implementable device that can be used with QD emitters.

Our protocol is based on the two optical transitions of a lambda system, given by a singly charged QD (trion) in an in-plane magnetic field (Voigt configuration), cf. Fig. 1(a). In this configuration there are two allowed linearly polarized optical transitions that decay at the same rate [31], while the two optical ground states are coupled by a spin-flip rate. Experiments have shown that it is possible to operate in a regime (depending on the Zeeman splitting, sample temperature, and the cotunneling rates) where the spin-flip process is dominated by single-acoustic-phonon mediated transitions [32,33], which is in good agreement with theoretical predictions [34–36]. We note that the coherence properties of the emitted phonons are inherited from the coherence of the spin. In many QD experiments the spin coherence appears not to be limited by phonon mediated relaxation processes [37], leading to the emission of incoherent phonons. This would limit the usefulness of these phonons as a coherent quantum bus, mediating interaction between emitters. However, recently progress has been made towards increasing the spin-coherence times [38] and the ultimately limiting process remains to be determined, especially when operating at millikelvin temperatures. The emitter is

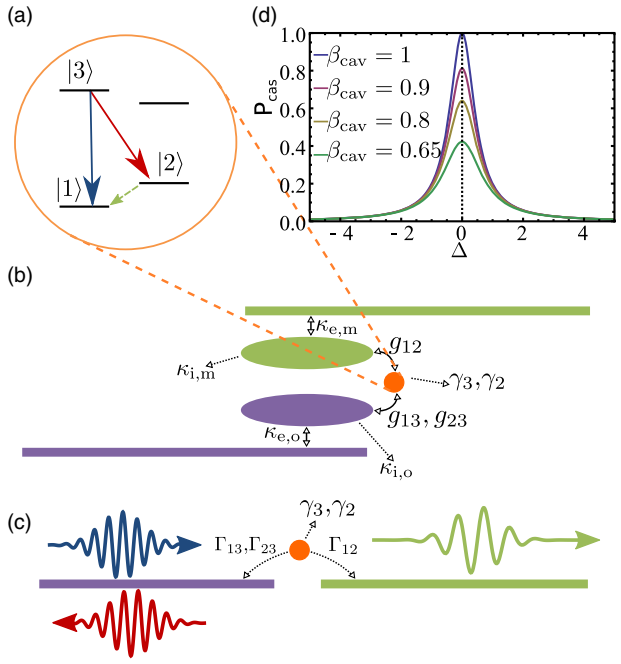

FIG. 1. Operational principle of the deterministic single-photon–single-phonon cascade. (a) Level structure of a singly charged exciton in a magnetic field in Voigt configuration. The optical transitions between states $|1\rangle$ and $|3\rangle$ and states $|2\rangle$ and $|3\rangle$ form a lambda system, indicated by the solid arrows. Furthermore, the two ground states, $|1\rangle$ and $|2\rangle$, are coupled to each other via a single-phonon-mediated transition, indicated by the dashed arrow. (b) Schematic of the desired OM-circuit functioning as a heralded single-phonon source, which is deterministically triggered by a single photon. The photonic (phononic) waveguide, shown in purple on the bottom (green at the top), couples the single photons (phonons) into and out of the OM-cavity modes (middle) at the rate $\kappa_{e,o}$ ($\kappa_{e,m}$). The QD couples to the photonic and the colocalized phononic mode of the OM cavity with the rates g_{13}, g_{23}, and g_{12} and to the loss modes in the photonic and phononic environments with rates γ_3 and γ_2. (c) The schematic of the effective OM circuit for the parameter regime discussed in the text and with the relevant rates indicated. The incident photon (blue wave packets) triggers the outgoing photon-phonon cascade (red wave packet and green wave packet). (d) The success probability of initializing the photon-phonon pair by a single photon incident on the trigger transition as a function of detuning of the trigger photon, $\Delta = \omega_{tr} - \omega_{13}$, for several values of the cavity-β factors, $\beta_{cav} = (\Gamma_{13} + \Gamma_{23})/(\Gamma_{13} + \Gamma_{23} + \gamma_3)$.

embedded in an OM circuit shown schematically in Fig. 1(b). A semi-infinite photonic (phononic) waveguide couples the single photons (phonons) into and out of the OM circuit. The photonic and phononic waveguides each couple to their respective mode of the OM cavity at the rates denoted $\kappa_{e,o}$ and $\kappa_{e,m}$. All relevant rates are indicated in Fig. 1(b) and controlling their relative magnitudes offer a wide range of design possibilities. For the remainder of this Letter, we will focus on just one of these different realizations, which is well suited for the deterministic generation of single phonons. We consider the case where both cavity modes are in the overcoupled regime, meaning that the resonator loss is dominated by the coupling to the waveguide mode, $\kappa_{e,o}(\kappa_{e,m}) \gg \kappa_{i,o}(\kappa_{i,m})$ [25]. Thus, the intrinsic cavity loss rates, $\kappa_{i,o}$ and $\kappa_{i,m}$, can be neglected in the following. The emitter-resonator coupling is in the bad cavity but large cooperativity regime, i.e., $\kappa_{e,o} \gg g_{13}, g_{23}$ and $\kappa_{e,m} \gg g_{12}$ but $4(g_{13}^2 + g_{23}^2)/(\kappa_{e,o}\gamma_3) \gg 1$ and $2g_{12}^2/(\kappa_{e,m}\gamma_2) \gg 1$ [39]. In the bad cavity regime the influence of the cavity on an emitter close to resonance can be captured by a cavity-enhanced effective decay rate of the excited state into the cavity mode: $\Gamma_{12} = 2g_{12}^2/\kappa_{e,m}$, $\Gamma_{13} = 2g_{13}^2/\kappa_{e,o}$, and $\Gamma_{23} = 2g_{23}^2/\kappa_{e,o}$ [39]. Thus, the schematic in Fig. 1(b) simplifies to the effective circuit shown in Fig. 1(c) for the implementation we are considering here, cf. the Supplemental Material for the Hamiltonian of the system [40]. This is best described as an emitter coupled to unidirectional photonic and phononic reservoirs [46,47]. The single-frequency scattering coefficient for the elastic scattering of a trigger photon, ω_{tr}, incident on the $|3\rangle \rightarrow |1\rangle$ transition is given by

$$t_{tr} = \frac{\Delta - i(\Gamma_{13} - \Gamma_{23} - \gamma_3)/2}{\Delta + i(\Gamma_{13} + \Gamma_{23} + \gamma_3)/2}. \quad (1)$$

For the case of $\Gamma_{13} = \Gamma_{23} + \gamma_3$ and $\Delta = \omega_{tr} - \omega_{13} = 0$, i.e., when Γ_{13} is equal to the total decay rate into all other modes and the incident photon is on resonance and is narrow band compared to the QD transition, we see complete destructive interference of the light scattered into the OM circuit at the resonance frequency ω_{13}. Thus, the photon has to be scattered along one of the remaining available decay channels [48,49]. Consequently, the scattering coefficient for a trigger photon incident on the $|3\rangle \rightarrow |1\rangle$ transition to Raman scatter along the $|3\rangle \rightarrow |2\rangle$ transition is

$$t_{cas} = \frac{-i\sqrt{\Gamma_{13}\Gamma_{23}}}{\Delta + i(\Gamma_{13} + \Gamma_{23} + \gamma_3)/2}. \quad (2)$$

From Eq. (2) we calculate the success probability of initializing the single-photon–single-phonon cascade process, cf. Fig. 1(d), which approaches unity for large coupling efficiencies of the optical transitions. It is promising to note that recent experiments in photonic-crystal waveguides have shown that even for moderate enhancements of the waveguide mode, spontaneous-emission coupling efficiencies $\beta_{wg} > 98\%$ can be readily achieved [50]. This is largely the result of the strongly suppressed coupling to optical loss modes for QDs embedded in photonic-crystal membranes [51]. The incident and outgoing wave packets for the successful generation of a photon-phonon cascade from a single incident trigger photon is illustrated in Fig. 1(c).

Implementing the circuit in Fig. 1(b) requires an OM crystal that supports photonic and phononic band gaps at frequencies relevant to the optical transitions [2] and the Zeeman splitting [37] obtainable for the considered emitter,

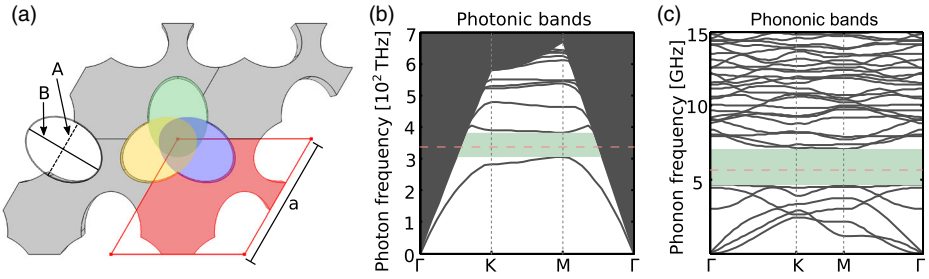

FIG. 2. Design of the OM-crystal membrane. (a) Illustration of the OM crystal with a single unit cell highlighted. The holes in the membrane consist of three overlapping ellipsoids, indicated by the three shaded regions, rotated by $2\pi/3$ with respect to one another. The lattice constant of the crystal is denoted by a and the minor and major axis of the ellipsoids are denoted by A and B. (b) The photonic band structure of the shamrock crystal with parameters $(a, A, B, L, d) = (300\ \text{nm}, 0.45a, 0.6a, 0.17a, 0.65a)$. The symmetries and the irreducible Brillouin zone of this crystal are discussed in the Supplemental Material. For the parameters used here we find a band gap for the TE-like slab modes in the frequency range 305 to 383 THz. (c) Phononic band structure for the same crystal parameters displaying a complete phononic band gap in the range 4.7 to 7.1 GHz. The horizontal dashed lines in (b) and (c) indicate the photonic and phononic resonance frequencies of the cavity modes shown in Fig. 1(b). The photonic resonance frequency was chosen to fall within the range of optical transitions of standard InGaAs QDs and the phononic resonance frequency corresponds to a Zeeman energy splitting achievable in standard cryomagnet systems.

i.e., InGaAs QDs. The OM crystal we propose [shown in Fig. 2(a)] consists of a hexagonal array of holes, separated by the lattice constant $a = 300$ nm etched into a GaAs membrane of thickness $d = 0.65a$. Each hole is made up by three overlapping ellipses rotated by $2\pi/3$ with respect to one another. The minor and major axes of the ellipse are given by $A = 0.45a$ and $B = 0.6a$, respectively. The center of each ellipse is shifted outwards along its major axis by $L = 0.17a$ resulting in a final shape that is reminiscent of a shamrock, cf. Fig. 2(a). This leads to a reduction of the crystal symmetry compared to conventional photonic [2] and previous OM crystals [6], cf. the Supplemental Material for more information on the reduction of the crystal symmetry [40]. A similar structure has been investigated for its photonic properties [52].

The photonic band diagram for modes with TE-like symmetry is shown in Fig. 2(b). The lightly shaded region in the center indicates the in-plane band gap and the dashed line marks the position of the optical transitions within the band gap. The dark shaded region at the sides and the top of Fig. 2(b) indicates the continuum of leaky radiation modes, i.e., modes that are not confined to the membrane. For simulations of the phononic bands (see Supplemental Material for details) we consider the modes of all symmetries, cf. Fig. 2(c), taking into account the anisotropy of the elastic constants of gallium arsenide. In the phononic band structure there are no leaky modes, as all modes are confined to the membrane. Thus, contrary to the photonic case, the phononic band diagrams exhibit a complete band gap. This has promising implications for the control of single-phonon mediated transitions as they can be completely suppressed within the band gap, where the phononic density of states drops to zero. For our proposal this means that the coupling efficiency of the $|2\rangle \rightarrow |1\rangle$ transition to the phononic cavity mode is only limited by the probability to decay through a single-phonon process, as opposed to other spin-relaxation processes such as cotunneling [33] and multiphonon effects [34,35,53]. This differs from the coupling efficiencies in photonic systems, where in addition to the probability of the emitter decaying through a single-photon process, the coupling efficiency is limited by the coupling to nonguided radiation modes [50]. Nonetheless, completely analogous to optical emitters in photonic crystals, the coupling rate to the target mode can be enhanced by increasing the local density of mechanical states through the use of defect modes.

We now demonstrate some of the different types of defect modes employed for the realization of the proposal. In Fig. 3(a) we show a purely phononic waveguide formed by replacing a row of shamrock holes by circular holes. This waveguide exhibits a gap at the relevant photonic frequencies, and corresponds to the waveguide at the top of Fig. 1(b). It allows introducing a large $\kappa_{e,m}$, by bringing it close to the cavity, while leaving the optical cavity modes largely unaffected. A different waveguide design is obtained by removing a row of shamrock holes and scaling the spacing between the remaining adjacent rows of holes to $\sqrt{3}aW$. The modes for a waveguide width of $W = 0.58$ are shown in Fig. 3(b). This waveguide supports both a photonic and a phononic mode with band edges close to the respective transition frequencies of the emitter. The band edges of both modes shift up in frequency when reducing the width of the waveguide, eventually leading to a dual band gap at the frequencies relevant for the emitter for $W = 0.52$. This makes the waveguide in Fig. 3(b) well suited for the design of heterostructure cavities, that simultaneously support modes at the desired photonic and phononic frequencies [6,8], which corresponds to the OM cavity drawn in Fig. 1(b). One realization of such a cavity and the mode profiles of the optical and the

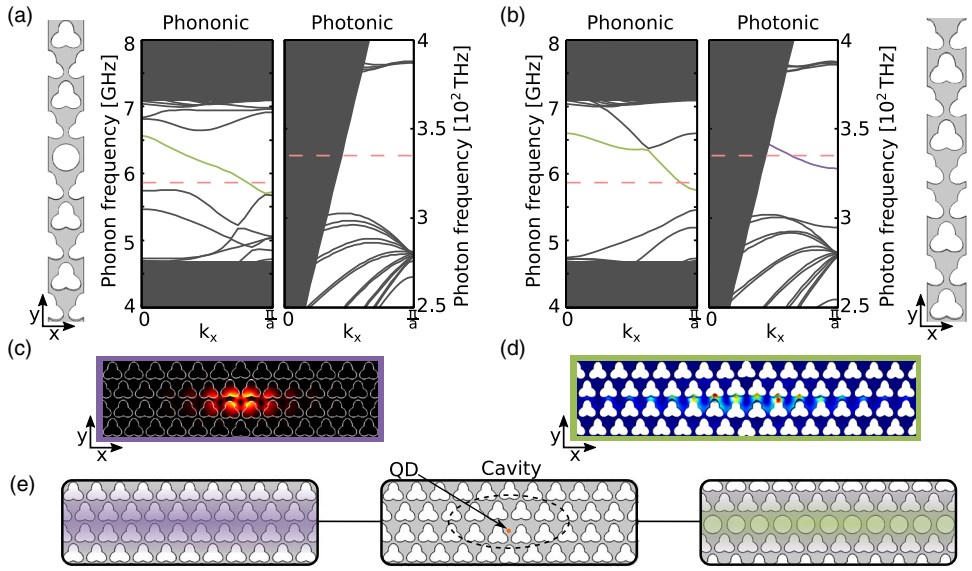

FIG. 3. Waveguides and cavities in OM-crystal membrane structure. (a) A phononic waveguide formed by replacing a row of shamrock holes by circular holes with radius $= 0.39a$ (left). This waveguide supports a mode at the relevant phonon frequency (middle) while exhibiting a gap at the relevant photonic frequencies (right). (b) A different waveguide design, where a row of shamrock holes is removed and not replaced by anything. The gap between the two sides of the crystal is reduced to $0.58a\sqrt{3}$, referred to as a $W = 0.58$ waveguide (right). This waveguide supports both a photonic (middle) and a phononic (left) mode. The band edges of the waveguide modes (green and purple solid lines) shift up in frequency when reducing the width of the waveguide, leaving the transition in a band gap for $W = 0.52$. Combining sections of $W = 0.52$ with a 2-period long section of $W = 0.58$ a heterostructure cavity is formed. (c) The modulus squared, $|E|^2$, profile of an optical resonance at 337 THz. (d) The displacement of a mechanical resonance at 5.9 GHz. (e) The three optomechanical circuit elements needed to implement the schematic in Fig. 1(b). The QD is positioned in the OM-cavity coupling to the two modes shown in (c) and (d), cf. the Supplemental Material for an example of how these circuit elements might be combined [40].

mechanical modes are shown in Figs. 3(c) and 3(d), cf. the Supplemental Material for numerical simulations of the radiative coupling efficiency of a dipole to the optical mode [40]. In Fig. 3(e) the circuit elements needed to assemble the circuit sketched in Fig. 1(b) are collected. The two types of waveguides discussed suffice to realize the OM circuit sketched in Figs. 1(b) and 1(c) by ensuring that the cavity's dominant mechanical loss rate, $\kappa_{e,m}$, is to the purely phononic waveguide in Fig. 3(a); i.e., the mechanical cavity mode only couples very weakly to the waveguide in Fig. 3(b). However, similar design ideas have been used to realize purely photonic waveguide defects in the same OM crystal, cf. the Supplemental Material for more information on this design [40]. Thus, this new type of OM crystal is a versatile platform for on-chip optomechanics.

In this Letter, we have demonstrated a scheme for single-phonon generation in an optomechanical crystal. The scheme is based on a QD embedded in a membrane GaAs nanostructure whose periodic properties lead to simultaneous photonic and phononic band gaps, allowing us to control optical and acoustical interaction processes in the emitter. We have designed waveguides and cavities for both photons and phonons by introducing different types of crystal defects. Throughout the work the focus has been on designing structures that can be experimentally realized within the current scope of gallium arsenide nanofabrication.

Finally, we note that other solid-state systems, such as silicon-vacancy centers in diamond, appear to have spin-coherence times limited by single-phonon mediated relaxation processes [54,55]. In addition to enhancing the spin coherence of such a system it also becomes possible for the phonons to act as a coherent on-chip quantum bus, which can couple several emitters [16] or act as a transducer from the optical to the microwave regime [56,57]. When exploiting the type of three-level system discussed here, the resulting photon-phonon cascade can be used to implement the DLCZ (Duan, Lukin, Cirac, and Zoller) protocol [58]. Other possible applications include the creation of vibration amplification by stimulated emission of radiation [59,60].

We would like to thank Alisa Javadi, Anders Sørensen, Richard Warburton, Petru Tighineanu, Sahand Mahmoodian, and Tommaso Pregnolato for helpful discussions. We gratefully acknowledge financial support from the Danish Council for Independent Research (Natural Sciences and Technology and Production Sciences) and the European Research Council (ERC Consolidator Grant—ALLQUANTUM).

*immo.soellner@unibas.ch
Present address: The University of Basel, Basel, Switzerland.

[1] J. D. Joannopoulos, S. G. Johnson, J. N. Winn, and R. D. Meade, *Photonic Crystals: Molding the Flow of Light*, 2nd ed. (Princeton University Press, Princeton, 2011).
[2] P. Lodahl, S. Mahmoodian, and S. Stobbe, Rev. Mod. Phys. **87**, 347 (2015).
[3] T. Gorishnyy, M. Maldovan, C. Ullal, and E. Thomas, Phys. World **18**, 24 (2005).
[4] M. Maldovan and E. L. Thomas, Appl. Phys. Lett. **88**, 251907 (2006).
[5] M. Eichenfield, J. Chan, R. M. Camacho, K. J. Vahala, and O. Painter, Nature (London) **462**, 78 (2009).
[6] A. H. Safavi-Naeini and O. Painter, Opt. Express **18**, 14926 (2010).
[7] S. Mohammadi, A. A. Eftekhar, A. Khelif, and A. Adibi, Opt. Express **18**, 9164 (2010).
[8] A. H. Safavi-Naeini and O. Painter, New J. Phys. **13**, 013017 (2011).
[9] M. Schmidt, V. Peano, and F. Marquardt, New J. Phys. **17**, 023025 (2015).
[10] J. Chan, T. P. M. Alegre, A. H. Safavi-Naeini, J. T. Hill, A. Krause, S. Gröblacher, M. Aspelmeyer, and O. Painter, Nature (London) **478**, 89 (2011).
[11] J. D. Cohen, S. M. Meenehan, G. S. MacCabe, S. Gröblacher, A. H. Safavi-Naeini, F. Marsili, M. D. Shaw, and O. Painter, Nature (London) **520**, 522 (2015).
[12] R. Riedinger, S. Hong, R. A. Norte, J. A. Slater, J. Shang, A. G. Krause, V. Anant, M. Aspelmeyer, and S. Gröblacher, Nature (London) **530**, 313 (2016).
[13] P. Rabl, P. Cappellaro, M. V. Gurudev Dutt, L. Jiang, J. R. Maze, and M. D. Lukin, Phys. Rev. B **79**, 041302 (2009).
[14] O. Arcizet, V. Jacques, A. Siria, P. Poncharal, P. Vincent, and S. Seidelin, Nat. Phys. **7**, 879 (2011).
[15] I. Wilson-Rae, P. Zoller, and A. Imamoğlu, Phys. Rev. Lett. **92**, 075507 (2004).
[16] S. D. Bennett, N. Y. Yao, J. Otterbach, P. Zoller, P. Rabl, and M. D. Lukin, Phys. Rev. Lett. **110**, 156402 (2013).
[17] P. Ovartchaiyapong, K. W. Lee, B. A. Myers, and A. C. B. Jayich, Nat. Commun. **5**, 4429 (2014).
[18] A. Barfuss, J. Teissier, E. Neu, A. Nunnenkamp, and P. Maletinsky, Nat. Phys. **11**, 820 (2015).
[19] E. R. MacQuarrie, T. A. Gosavi, N. R. Jungwirth, S. A. Bhave, and G. D. Fuchs, Phys. Rev. Lett. **111**, 227602 (2013).
[20] I. Yeo, P.-L. de Assis, A. Gloppe, E. Dupont-Ferrier, P. Verlot, N. S. Malik, E. Dupuy, J. Claudon, J.-M. Gérard, A. Auffèves, G. Nogues, S. Seidelin, J.-P. Poizat, O. Arcizet, and M. Richard, Nat. Nanotechnol. **9**, 106 (2013).
[21] M. Montinaro, G. Wüst, M. Munsch, Y. Fontana, E. Russo-Averchi, M. Heiss, A. Fontcuberta I Morral, R. J. Warburton, and M. Poggio, Nano Lett. **14**, 4454 (2014).
[22] J. I. Colless, X. G. Croot, T. M. Stace, A. C. Doherty, S. D. Barrett, H. Lu, A. C. Gossard, and D. J. Reilly, Nat. Commun. **5**, 3716 (2014).
[23] K. D. Jahnke, A. Sipahigil, J. M. Binder, M. W. Doherty, M. Metsch, L. J. Rogers, N. B. Manson, M. D. Lukin, and F. Jelezko, New J. Phys. **17**, 043011 (2015).
[24] M. R. Vanner, M. Aspelmeyer, and M. S. Kim, Phys. Rev. Lett. **110**, 010504 (2013).
[25] C. Galland, N. Sangouard, N. Piro, N. Gisin, and T. J. Kippenberg, Phys. Rev. Lett. **112**, 143602 (2014).
[26] H. Flayac and V. Savona, Phys. Rev. Lett. **113**, 143603 (2014).
[27] M. Aspelmeyer, T. J. Kippenberg, and F. Marquardt, Rev. Mod. Phys. **86**, 1391 (2014).
[28] S. M. Meenehan, J. D. Cohen, S. Gröblacher, J. T. Hill, A. H. Safavi-Naeini, M. Aspelmeyer, and O. Painter, Phys. Rev. A **90**, 011803(R) (2014).
[29] We refer to Ref. [30] for a discussion about what constitutes narrow bandwidth for the incident photon and the role of dephasing in the coherent scattering regime.
[30] I. Söllner, S. Mahmoodian, S. L. Hansen, L. Midolo, A. Javadi, G. Kiršanskė, T. Pregnolato, H. El-Ella, E. H. Lee, J. D. Song, S. Stobbe, and P. Lodahl, Nat. Nanotechnol. **10**, 775 (2015).
[31] D. Press, T. D. Ladd, B. Zhang, and Y. Yamamoto, Nature (London) **456**, 218 (2008).
[32] M. Kroutvar, Y. Ducommun, D. Heiss, M. Bichler, D. Schuh, G. Abstreiter, and J. J. Finley, Nature (London) **432**, 81 (2004).
[33] J. Dreiser, M. Atatüre, C. Galland, T. Müller, A. Badolato, and A. Imamoğlu, Phys. Rev. B **77**, 075317 (2008).
[34] A. V. Khaetskii and Y. V. Nazarov, Phys. Rev. B **64**, 125316 (2001).
[35] L. M. Woods, T. L. Reinecke, and Y. Lyanda-Geller, Phys. Rev. B **66**, 161318(R) (2002).
[36] V. N. Golovach, A. Khaetskii, and D. Loss, Phys. Rev. Lett. **93**, 016601 (2004).
[37] R. J. Warburton, Nat. Mater. **12**, 483 (2013).
[38] D. Brunner, B. D. Gerardot, P. A. Dalgarno, G. Wüst, K. Karrai, N. G. Stoltz, P. M. Petroff, and R. J. Warburton, Science **325**, 70 (2009).
[39] P. R. Rice and H. J. Carmichael, IEEE J. Quantum Electron. **24**, 1351 (1988).
[40] See Supplemental Material at http://link.aps.org/supplemental/10.1103/PhysRevLett.116.234301 for more information, which includes Refs. [41–45].
[41] K. Sakoda, *Optical Properties of Photonic Crystals*, 2nd ed., edited by W. Rhodes (Springer, Berlin, Heidelberg, New York, 2005).
[42] R. Mirman, *Point Groups, Space Groups, Crystals, Molecules* (World Scientific, Singapore, 1999).
[43] T. Terzibaschian and R. Enderlein, Phys. Status Solidi (b) **133**, 443 (1986).
[44] L. C. Andreani and D. Gerace, Phys. Rev. B **73**, 235114 (2006).
[45] S. G. Johnson and J. D. Joannopoulos, Opt. Express **8**, 173 (2001).
[46] E. Rephaeli and S. Fan, Photon. Res. **1**, 110 (2013).
[47] T. C. Ralph, I. Söllner, S. Mahmoodian, A. G. White, and P. Lodahl, Phys. Rev. Lett. **114**, 173603 (2015).
[48] M. Bradford, K. C. Obi, and J. T. Shen, Phys. Rev. Lett. **108**, 103902 (2012).
[49] I. Shomroni, S. Rosenblum, Y. Lovsky, O. Bechler, G. Guendelman, and B. Dayan, Science **345**, 903 (2014).
[50] M. Arcari, I. Söllner, A. Javadi, S. Lindskov Hansen, S. Mahmoodian, J. Liu, H. Thyrrestrup, E. H. Lee, J. D. Song, S. Stobbe, and P. Lodahl, Phys. Rev. Lett. **113**, 093603 (2014).

[51] Q. Wang, S. Stobbe, and P. Lodahl, Phys. Rev. Lett. **107**, 167404 (2011).
[52] F. Wen, S. David, X. Checoury, M. El Kurdi, and P. Boucaud, Opt. Express **16**, 12278 (2008).
[53] M. Trif, P. Simon, and D. Loss, Phys. Rev. Lett. **103**, 106601 (2009).
[54] L. J. Rogers, K. D. Jahnke, M. H. Metsch, A. Sipahigil, J. M. Binder, T. Teraji, H. Sumiya, J. Isoya, M. D. Lukin, P. Hemmer, and F. Jelezko, Phys. Rev. Lett. **113**, 263602 (2014).
[55] B. Pingault, J. N. Becker, C. H. H. Schulte, C. Arend, C. Hepp, T. Godde, A. I. Tartakovskii, M. Markham, C. Becher, and M. Atatüre, Phys. Rev. Lett. **113**, 263601 (2014).
[56] M. Davanço, J. Chan, A. H. Safavi-Naeini, O. Painter, and K. Srinivasan, Opt. Express **20**, 24394 (2012).
[57] J. Bochmann, A. Vainsencher, D. D. Awschalom, and A. N. Cleland, Nat. Phys. **9**, 712 (2013).
[58] L. M. Duan, M. D. Lukin, J. I. Cirac, and P. Zoller, Nature (London) **414**, 413 (2001).
[59] K. V. Kepesidis, S. D. Bennett, S. Portolan, M. D. Lukin, and P. Rabl, Phys. Rev. B **88**, 064105 (2013).
[60] J. Kabuss, A. Carmele, T. Brandes, and A. Knorr, Phys. Rev. Lett. **109**, 054301 (2012).